PAPER

Does the Larkin length exist?

IOP Publishing Modelling and Simulation in Materials Science and Engineering

Modelling Simul. Mater. Sci. Eng. **32** (2024) 035007 (18pp) https://doi.org/10.1088/1361-651X/ad2543

Does the Larkin length exist?

David Rodney[1,*], Pierre-Antoine Geslin[2], Sylvain Patinet[3], Vincent Démery[4,5] and Alberto Rosso[6]

[1] Institut Lumière Matière, Univ. Lyon, CNRS, Université Claude Bernard Lyon 1, 69622 Villeurbanne, France
[2] MATEIS, Univ. Lyon, CNRS, INSA Lyon, Université Claude Bernard Lyon 1, 69100 Villeurbanne, France
[3] PMMH, CNRS, ESPCI Paris, Université PSL, Sorbonne Université, Université de Paris, 75005 Paris, France
[4] Gulliver, CNRS, ESPCI Paris, Université PSL, 75005 Paris, France
[5] Laboratoire de Physique, CNRS, ENS de Lyon, Université de Lyon, 69364 Lyon, France
[6] LPTMS, CNRS, Université Paris-Saclay, 91405 Orsay, France

E-mail: david.rodney@univ-lyon1.fr

Received 12 December 2023; revised 23 January 2024
Accepted for publication 1 February 2024
Published 13 February 2024

Abstract

The yield stress of random solid solutions is a classic theme in physical metallurgy that currently attracts a renewed interest in connection to high entropy alloys. Here, we revisit this subject using a minimal dislocation dynamics model, where a dislocation is represented as an elastic line with a constant line tension embedded in the stochastic stress field of the solutes. Our exploration of size effects reveals that the so-called Larkin length (L_c) is not a length scale over which a dislocation can be geometrically decomposed. Instead, L_c is a crossover length scale marking a transition in dislocation behavior identifiable in at least three properties: (1) below L_c, the dislocation is close to straight, aligned in a single energy valley, while above L_c, it roughens and traverses several valleys; (2) the yield stress exhibits pronounced size-dependence below L_c but becomes size-independent above L_c; (3) the power-spectral density of the dislocation shape changes scaling at a critical wavelength directly proportional to L_c. We show that for white and correlated stress noises, L_c and the thermodynamic limit of the yield stress can be predicted using Larkin's model, where the noise dependence in the glide direction is neglected. Moreover, we show that our analysis is relevant beyond the minimal line tension model by comparison with atomic-scale simulations. Finally, our work suggests a practical approach

* Author to whom any correspondence should be addressed.

for predicting yield stresses in atomistic models of random solid solutions, which only involves small-scale atomistic simulations below L_c.

Keywords: plasticity, dislocation dynamics, depinning transition, solid solution strengthening

1. Introduction

Throughout this career, Ladislas Kubin has been instrumental in the development of a physical approach of crystalline plasticity [1], reflected in his book [2] and pioneering contributions in electron microscopy observations of [3], Portevin-Le Châtelier effect [4, 5], and crystal plasticity models [6, 7]. He is also one of the fathers of dislocation dynamics (DD) simulations. With Gilles Canova, who left us too early, they were among the first to envision the potential power of the simulation of dislocation ensembles in 3 dimensions (3D). In contrast, at the time, DD simulations were performed in 2 dimensions (2D) [8]. This endeavor started at the end of the 1980's [9] with highly unstable dislocations illustrated in figure 1(a). Nevertheless, it led to ever more accurate and larger-scale models of 3D plasticity, an example of which is shown in figure 1(b).

The reason dislocations are so messy in figure 1(a) is that the line tension was not included in the simulations. Adding this term [11] allowed to stabilize the dislocation lines and opened the way to realistic 3D simulations accounting for both short- and long-range interactions along dislocations and between dislocations as illustrated in figure 1(b).

At the other end of the spectrum of complexity in dislocation models lies the line tension model, where all long-range elastic interactions are neglected, and only the short-range line tension is kept. This minimal model has been highly beneficial in analyzing dislocation processes, including junction formation and breaking [12, 13] and glide through random fields of localized obstacles [14, 15], as well as to measure stresses in *in situ* microscopy [16]. The line tension model is also helpful in studying plasticity in random solid solutions [17]. A dislocation is then represented by a function $y = h(x)$ in its (x, y) glide plane where the solutes produce a random stress field $\tau_R(x, y)$. This field is usually taken as a random white noise, although we have recently shown that it is spatially correlated [18, 19]. The overdamped equation of DD reads:

$$B\partial_t h = T\partial_x^2 h + b\tau_R\left(x, h\left(x\right)\right) + b\tau_A, \tag{1}$$

in the limit of small curvatures typical of solid solutions (B is a damping coefficient, T the line tension, b the Burgers vector and τ_A the applied stress). Introducing a small length scale a, which physically corresponds to the lattice parameter, the Burgers vector or the correlation length of the stress noise, distances can be scaled by a, stresses by T/ba and time by Ba/T, to re-write the equation of dynamics as:

$$\partial_t h = \partial_x^2 h + R\left(x, h\right) + A. \tag{2}$$

In this scaled representation, the dislocation line tension is a constant equal to 1, the solutes are modeled by a random noise R with zero mean and the applied stress becomes a constant, A, which we will call force, as customarily done in the field of disordered elastic media. This equation is the quenched Edwards–Wilkinson (qEW) equation in $d = 1 + 1$ dimensions [20–22], which is well-known for presenting a depinning transition: when the driving force A is small compared to the noise R, the elastic line finds an equilibrium configuration and is

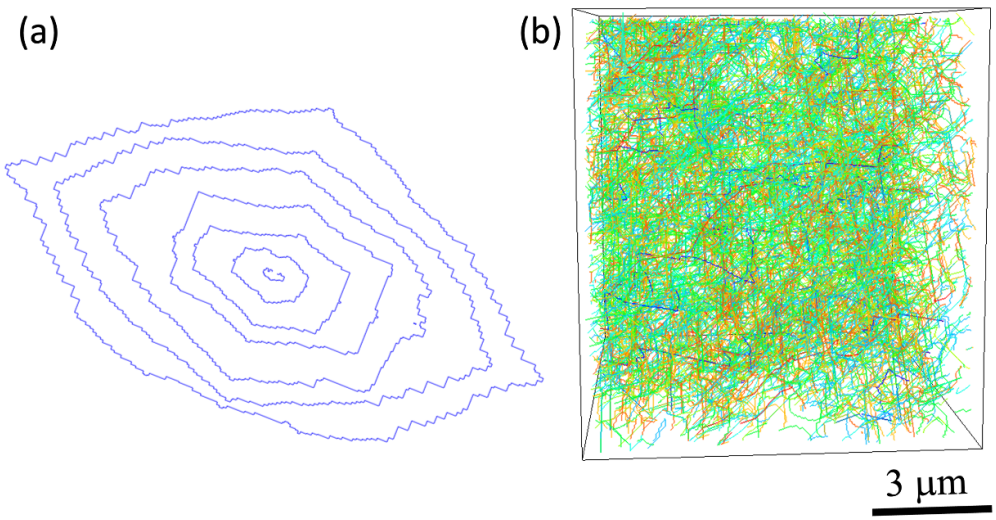

Figure 1. Illustrations of (a) a very first dislocation dynamics simulation in 3D of a Frank-Read source and (b) a state-of-the-art simulation of plasticity in copper. Both simulations were kindly performed by Ronan Madec using the 3D simulation code MobiDiC [10].

pinned, while the line moves indefinitely with a finite average velocity above a critical driving force, A_c. In the context of dislocations, this critical force corresponds to the critical resolved shear stress or simply the yield stress. The qEW equation has been extensively used to study the dynamics of surface roughening in a random noise [23–25] and other properties, such as size effects and distributions of critical forces [26]. However, the dependence of the critical force on the amplitude of the noise, which in the context of solid solution strengthening corresponds to the dependence of the yield stress on the concentration and solute mismatch [27], has been addressed in much less details [28] and is the subject of the present work.

In honor of Ladislas Kubin, we will examine how the minimal line tension model helps us understand how dislocations behave in the presence of a random field of solutes. In particular, we will discuss the existence and properties of the so-called Larkin length, denoted L_c, which was originally introduced by Larkin and Ovchinninkov in the context of superconductors [29, 30]. In plasticity, the Larkin length marks a transition between short dislocations that are weakly pinned and almost straight due to their line tension and long dislocations that are strongly pinned by the disorder. How to determine L_c is yet a matter of debate. In the plasticity community [31–33], L_c is often defined from an equilibrium between line tension and random noise on a bulge of length L_c. This definition has, however, been called into question [28, 34, 35] since close to the critical stress, the line is known to be rough on all length scales (a property recognized early on by Ladislas Kubin [36]) and thus should not be decomposable into a succession of bow-outs with a single length scale L_c as some theoretical treatments imply [37, 38]. Moreover, we have recently shown that this definition yields an incorrect scaling in the presence of a correlated noise [28].

We will show here that L_c is best defined by looking at the size dependence of the yield stress, which transits from a strongly length-dependent regime below L_c to a length-independent regime above L_c. In other words, L_c is the characteristic size at which the yield

stress reaches its thermodynamic limit. We will see that equivalently, L_c is the size above which the so-called Larkin model, where finite correlations in the glide direction are neglected, ceases to be valid, as proposed in [39].

We point out that the motion of an elastic manifold in a random noise holds significance across various applications, ranging from geophysics and magnetic transitions to phenomena like the spreading of water droplets on dirty surfaces and vortex motion in superconductors [40]. Therefore, clarifying the concept of the Larkin length has relevance beyond the particular case of plasticity.

2. Methodology

To study a size effect on the dislocation yield stress and to approach a thermodynamic limit, we need to increase simultaneously the dislocation length and glide distance [15, 25, 26]. To this end, we will consider square cells in the (x, y) glide plane of side $L_x = L_y = L$, with periodic boundary conditions in both the x- and y-directions [28], see an illustration in the inset of figure 2. To implement equation (2) numerically, we discretize the $L \times L$ cell on a square lattice with a spacing a. The latter is used as unit length such that $L = N$ is an integer. The dislocation line is represented by a discrete set of heights, $\{h_n\}_{n\in[1,L]}$ with $h_n = h(na)$. In the first part of the paper (section 3), we consider an uncorrelated Gaussian noise R, with zero mean and standard deviation ΔR. The noise is generated on the square grid and is linearly interpolated in the glide direction (splines could also be used with no marked effect [25]). Effectively, the noise is thus correlated over a distance a in the y-direction.

Since we are interested in equilibrium configurations below A_c and not in the dynamics above A_c, we accelerate convergence to equilibrium using a quenched dynamics algorithm [41]. Although specific algorithms have been developed to efficiently determine A_c [23, 42], for the purpose of the present study, a simple quasi-static algorithm has proved sufficient: A is increased from 0 in small increments ($\Delta R/100$), and equilibrium configurations are obtained between each increment using quenched dynamics. The critical force A_c is reached when the dislocation line traverses the simulation cell, i.e. when its average position moves by a distance $> L$ without finding an equilibrium. Calculations are repeated in 100 different random cells to obtain statistically relevant averages.

3. Uncorrelated noise

3.1. Yield-stress dependence on noise amplitude

We start by modeling the effect of the solutes on the dislocation as a random white noise force field of standard deviation (or amplitude) ΔR. Figure 2 shows the result of DD simulations in square cells of size $L = 128,\ 512,\ 2048$. A extensive range of noise amplitudes ΔR was considered, spanning seven orders of magnitude. In this graph, we can distinguish three regions that are briefly presented here.

- **Region I**: At small ΔR, the critical force increases linearly, as $A_c \propto \Delta R$, as shown by the fit in figure 2. This region is characterized by strong finite size effects: (i) for a given ΔR, the critical force decreases with the system size, (ii) the range of values of ΔR in Region I decreases when L increases (e.g. in figure 2 there is no Region I for $L = 2048$). In Region I, the line tension dominates the stress noise. As we will see below, the dislocation remains inside a band of width a, corresponding to the disorder's correlation length in the glide

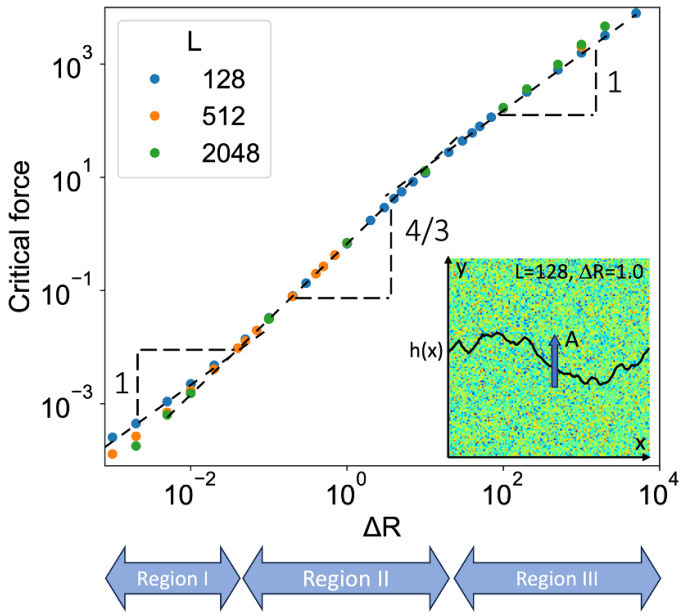

Figure 2. Average critical force as a function of noise amplitude computed in square cells $L \times L$ with different sizes indicated in the legend. The inset shows an example of critical configuration in Regime II.

direction. Indeed, within a, the random force can change sign at most once. This length corresponds to a single valley in the disorder energy landscape. Hence, Region I ends when the dislocation line starts to visit more than one valley.

- **Region II**: At intermediate ΔR, the critical force increases as $A_c \propto \Delta R^{4/3}$ as seen from the fit in figure 2. At a given ΔR, the critical force seems independent of the system size, although studies have shown that subdominant size effects exist [25, 26, 28]. In Region II, there is a balance between line tension and noise, and the dislocation is flexible enough to wander across several valleys to find strongly pinned configurations.
- **Region III**: At large ΔR, the critical force increases linearly again as $A_c \propto \Delta R$ as seen from the fit in figure 2. In Region III, the noise dominates the line tension, and the critical force is controlled by the largest noise peak (of order $\sim \Delta R\sqrt{2\ln L}$ for Gaussian variables) in the simulation cell.

In the literature, different names have been given to Regions I, II and III depending on the communities. In the physics community, Regions I and II are referred to as weak and strong pinning regions [43]. Tanguy and Vettorel first discussed the so-called weak-to-strong transition between Region I and II [44] using a perturbative approach and a minimal model of elastic lines. By way of contrast, in the plasticity community, Region I is usually not considered, Region II is referred to as weak (collective) pinning and Region III as strong (individual) pinning [33, 38, 45]. In the following, we will refer to Regions I, II, and III as weak pinning, strong collective pinning, and strong individual pinning, as proposed in [39]. Also, we will not consider Region III further because it is irrelevant for substitutional solid solutions that produce only a weak stress noise. Instead, we focus below on Regions I and II and on the weak-to-strong pinning transition between them. The latter was first discussed by Tanguy and

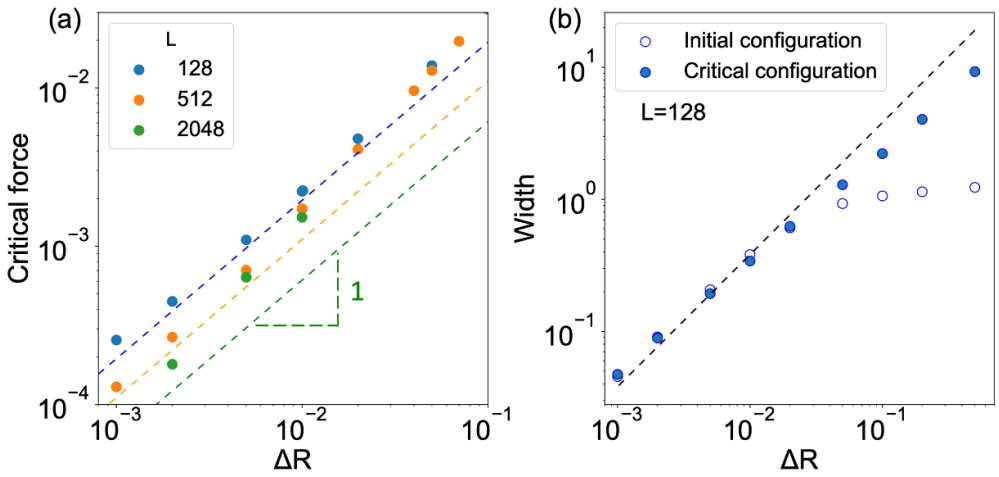

Figure 3. Average critical force (a) and dislocation width (b) as a function of noise amplitude ΔR. Panel (a) is a zoom of figure 2 in Region I. The dashed lines are predictions from Larkin model (equation (5)). In (b), the dislocation width ω is shown for $L = 128$ in the initial and critical configurations. The dashed line is the prediction from Larkin model (equation (8)).

Vettorel [44] for minimal models of elastic lines using a perturbative approach. Here, instead, we will use the full non-linear DD simulations.

3.2. Region I: weak pinning

3.2.1. Critical force and dislocation width. In this subsection, we discuss Region I, where the noise is weak and the dislocation behavior is dominated by the line tension. Figure 3(a) is a close-up of the critical force in this region, where we see clearly the linear dependence of the critical force on ΔR at low noise amplitudes. We also see that the extension of Region I depends strongly on L: the region of linear dependence extends up to about $\Delta R = 0.05$ for $L = 128$, 0.005 for $L = 512$ and no linear dependence is seen with $L = 2048$. Figure 3(b) shows the standard deviation of the dislocation height, often used to characterize the dislocation width in the glide direction:

$$\omega^2 = \frac{1}{L}\sum_{n=1}^{L}\left(h_n - \overline{h}\right)^2, \tag{3}$$

with $\overline{h} = (1/L)\sum_n h_n$. The width was computed for the initial configuration after relaxation from a straight line with no driving force and in the critical configuration, i.e. the last stable configuration before depinning. We see in figure 3(b) that at low noise ($\Delta R < 0.05$ for $L = 128$) the width is less than 1, i.e. less than the correlation length of the noise in the glide direction. The dislocation is thus located in a single valley between consecutive rows of random noise.

We also find that in Region I, the dislocation width does not evolve significantly between the initial and critical configurations: the dislocation may glide in the simulation cell to find the most resistant valley but retain an almost straight shape. Above $\Delta R > 0.05$ for $L = 128$, the width saturates near 1 in the initial configuration because the relaxation from a straight line does not allow the dislocation to explore more than one valley. However, in the critical

configuration, the width exceeds 1 because the dislocation develops large fluctuations and occupies several valleys. This is the classical roughening process characteristic of collective pinning [22, 39]. Comparing figures 3(a) and (b), we see that the end of Region I corresponds to both (1) when the critical force no longer varies linearly with ΔR and (2) when the width of the critical configuration exceeds 1 and is different from the width of the initial configuration.

3.2.2. Larkin model. Solving equation (2) is difficult because of the non-linear dependence of the noise on h. However, in Region I, the dislocation remains in a single valley where the noise varies slowly. We can thus attempt to model the dislocation in Region I by neglecting the variation of R in the y direction. This is the basis of Larkin's model [29, 30, 39], which assumes that for small excursions, the elastic manifold does not see that the correlation length is finite in the y direction.

With a constant noise in the y direction, the dislocation shape does not depend on the applied stress, which is consistent with the absence of width evolution in Region I observed in figure 3(b). Since the noise remains uncorrelated in the x direction, the total force on the dislocation is the sum of L independent Gaussian variables. The number of valleys in the cell scales with L, and if we assume that a different noise is sampled in each valley, the critical force corresponds to the maximum of L independent random variables of zero mean and standard deviation $\sqrt{L}\Delta R$. The latter is given by extreme value statistics [46]:

$$\langle A_c \rangle_I L \propto \left(\sqrt{L}\Delta R\right)\sqrt{\ln L} \tag{4}$$

i.e.

$$\langle A_c \rangle_I \propto \Delta R\sqrt{\frac{\ln L}{L}}. \tag{5}$$

The corresponding predictions are shown as dashed lines in figure 3(a), where we see a good agreement for $L = 128$ and 512. For $L = 2048$, the prediction is below the numerical data, which is consistent with the fact that for this dislocation length, Region I ends before $\Delta R = 10^{-3}$. We can thus conclude that in Region I, the dislocation acts as a rigid line, with a resistance controlled by the largest total noise experienced in the valleys of the energy disorder landscape.

3.2.3. Dislocation shape. As already seen from the finite dislocation widths in figure 3(b), the dislocation is not perfectly straight in Region I. This is also visible in figure 4, which shows the power spectral density (PSD) of the dislocation line in the initial and critical configurations. The PSD was obtained from a discrete Fourier transform of the dislocation heights using the convention: $\widehat{h}_k = (1/L)\sum_n h_n \exp(-jkn)$ with $k = m2\pi/L, m \in [0, L-1]$ and $\mathrm{PSD}(k) = \langle|\widehat{h}_k|^2\rangle$. Using again Larkin's assumption of a noise independent of h, we can take the Fourier transform of equation (2):

$$\langle|\widehat{h}_k|^2\rangle = \frac{\langle|\widehat{R}_k|^2\rangle}{k^4}, \tag{6}$$

for $k \neq 0$. Since the noise is uncorrelated along x, its power spectrum is a constant equal to $\langle|\widehat{R}_k|^2\rangle = \Delta R^2/L$ through Parseval's theorem. We thus expect a PSD:

$$\langle|\widehat{h}_k|^2\rangle = \frac{\Delta R^2}{Lk^4}. \tag{7}$$

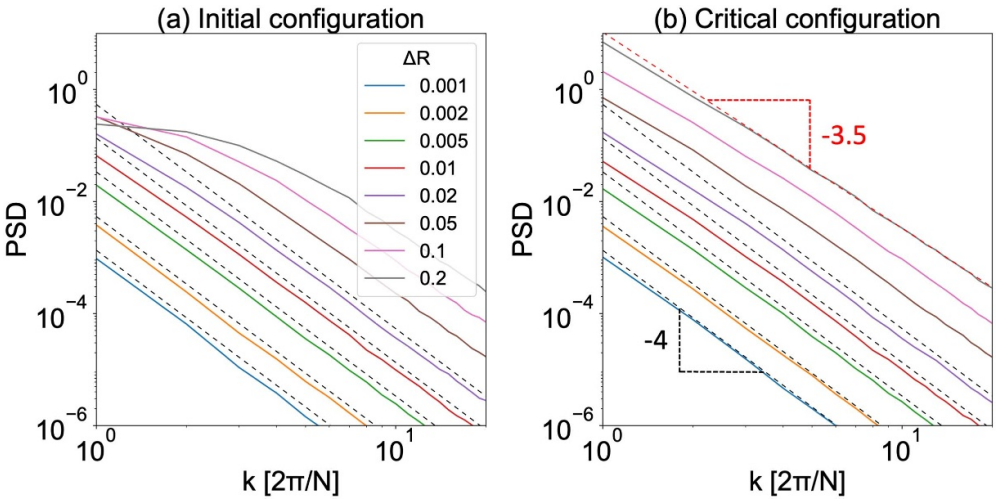

Figure 4. Power spectral density (PSD) of dislocation heights in the initial configuration (a) after relaxation from a straight line with no driving force and in the last stable configuration before A_c is reached (b). PSDs were averaged in 1000 cells with $L = 128$. The dashed black lines are predictions from Larkin model (equation (7)). The red dashed line is a numerical fit.

This prediction is shown as dashed lines in figure 4 where $L = 128$. Up to about $\Delta R = 0.02$, there is a good agreement with the numerical data. Moreover, we see that the PSD does not change between the initial and critical configurations, confirming that the dislocation behaves as a rigid, albeit noisy, line. Beyond $\Delta R = 0.02$, the PSD starts to level off in the initial configuration at small k, consistent with the saturation of the dislocation width in figure 3(b). Through the roughening process characteristic of Region II, the dislocation recovers a scale-free PSD in the critical configurations of figure 4(b), but with a smaller exponent: in Region I, the exponent is -4 while it is -3.5 in Region II, as seen by the dashed red line figure 4(b). The same exponent was obtained through large-scale simulations in [25]. We note that the roughening process occurs here upon increasing applied stress and does not require high temperatures in contrast with discussions in the literature [47].

Using again a Fourier transform, the dislocation width can be computed with Larkin's assumption:

$$\omega^2 = \sum_{k\neq 0} \langle |\widehat{h}_k|^2 \rangle = \frac{\Delta R^2}{L} \sum_{k\neq 0} \frac{1}{k^4} = \frac{\Delta R^2 L^3}{1440}, \tag{8}$$

where we have extended the sum over k to infinity and used the identity $\sum_{n=1}^{\infty} 1/n^4 = \pi^4/90$. The prediction was added to figure 3(b), with again a good agreement in Region I.

3.2.4. Larkin length. Based on the foregoing, we conclude that Region I of weak pinning is the region of validity of Larkin's assumption: the dislocation is close to straight, located in a single valley and sees an almost constant noise in the glide direction. As the noise amplitude increases, the width increases until the dislocation starts to visit more than one valley and feels the finiteness of the correlations along y.

For each L, we can thus define a critical noise amplitude above which Larkin's assumption is no longer valid. This corresponds to when the dislocation width reaches the size of a valley: $\omega_L(\Delta R_c) = 1$. Equivalently, for each ΔR, we can define a critical length above which Larkin's assumption is no longer valid. We propose to assimilate this length to the Larkin length L_c, which is thus defined as $\omega_{\Delta R}(L_c) = 1$. From equation (8), we have:

$$L_c = \left(\frac{1440}{\Delta R^2}\right)^{1/3}, \tag{9}$$

or reinserting the units:

$$L_c \approx 11.3 \left(\frac{aT^2}{b^2\langle\tau_R^2\rangle}\right)^{1/3}. \tag{10}$$

Following Larkin's pioneering work [29, 30, 39], we define here the Larkin length L_c as the length above which Larkin's assumption ceases to hold valid. It is worth noting that this definition diverges from an alternative interpretation of the Larkin length, which is deeply entrenched in the plasticity community [28, 31–33]. In this alternate view, it is postulated that the restoring force due to the line tension acting on a bulge of width a (the correlation length of the noise) is counterbalanced by the random force when the bulge length is the Larkin length, L_c. Both definitions (from the breakdown of Larkin model or from the bulge equilibrium) yield the same characteristic dependence $L_c \propto \langle\tau_R^2\rangle^{-1/3}$ for a white noise. However, this equivalence breaks down when we account for stress noise correlations along the dislocation line (see section 4).

The present definition of the Larkin length resembles the characteristic length ξ_c, introduced by W Curtin's group [37, 38]. In their work, dislocations are decomposed into straight segments of length ξ_c, which reside in regions of favorable fluctuations. Our analysis indeed confirms that segments below L_c are essentially straight. However, the PSDs of figure 4(b) do not show any peak that would indicate a dominant length scale. The dislocation thus cannot be geometrically decomposed into a succession of segments of a given length.

The Larkin length should therefore not be seen as a dominant length scale over which the dislocation can be decomposed but rather a crossover length scale. We have discussed above a crossover in the dislocation width, which exceeds the correlation length of the noise above L_c. This crossover can also be seen in the dislocation shape and its corresponding PSD. To show this, we present in figure 5 the same PSDs as in figure 4 but with the wave vectors scaled by $1/L_c$ and the PSDs by L_c/L. In this scaled representation, all PSDs collapse on master curves in both the initial and critical configurations. Moreover, both curves show two regimes with a crossover at $kL_c \simeq 64$ (this value is a numerical fit, corresponding to the intersection of the predicted $1/k^4$ and the fitted $1/k^{3.5}$ curves). Above $kL_c \simeq 64$, the PSDs follow the Larkin model, which, from equations (7) and (9), is expressed in scaled form as $\widetilde{\mathrm{PSD}} = 1440/k^4$, represented as a dashed black line in figures 5(a) and (b). Conversely, below $kL_c \simeq 64$, the PSDs saturate in the initial configurations and decrease as $1/k^{3.5}$ in the critical configurations. This crossover in the PSD scaling occurs at a characteristic wavelength $\lambda \sim \frac{2\pi}{64} L_c$, which is directly proportional to L_c.

3.3. Region II: strong collective pinning

As seen in figure 2, Region II is marked by a faster increase of the critical force with ΔR than in Region I. Moreover, the critical force, which depends intrinsically on the cell size in Region

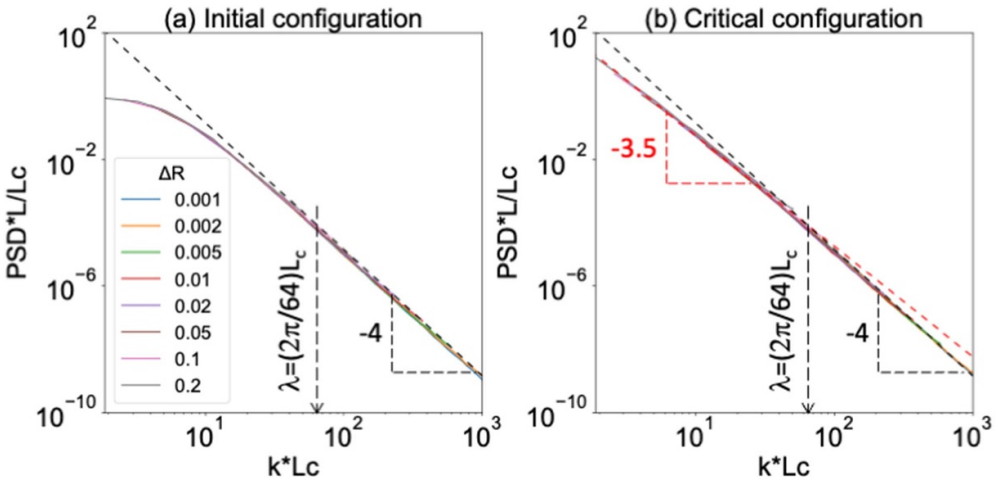

Figure 5. Scaled power spectral density (PSD) of dislocation heights in the (a) initial and (b) critical configurations. The same data are shown as in figure 4 but with the k-vectors scaled by $1/L_c$ and the PSDs scaled by L_c/L. The dashed black line in (a) and (b) is the prediction from Larkin model, which is expressed in scaled form as $\widetilde{\mathrm{PSD}} = 1440/\tilde{k}^4$. The red dashed line in (a) is a numerical fit.

I (see equation (5)), shows only a weak size effect in Region II. An alternative interpretation of Larkin length is thus that it is the characteristic length beyond which size effects stop and the yield stress reaches its thermodynamic limit. This limit thus corresponds to the yield stress value at the transition, i.e. $\langle A_c \rangle_I(L_c)$, since the dislocation length at the transition is the Larkin length. Neglecting the log-dependence in equation (5), we have:

$$\langle A_c \rangle_{II} \propto \frac{\Delta R}{\sqrt{L_c}}. \tag{11}$$

Since $L_c \propto 1/\Delta R^{2/3}$ from equation (9), we have:

$$\langle A_c \rangle_{II} \propto \Delta R^{4/3}, \tag{12}$$

which is the dependence of the critical force on ΔR observed in figure 2. This result is again in line with the Larkin model [29, 30, 39], which assumes that the critical force is given by the resistance of domains of size L_c, independently of the total length of the dislocation. This result might be surprising because it means that from the standpoint of the yield stress, a dislocation can be decomposed into segments of length L_c even if no dominant length scale emerges from the shape of the dislocation as discussed above. This also implies that in the PSDs of figure 4, the wavelengths larger than L_c do not contribute to the resistance of the dislocation.

From equations (9) and (12), we have $\langle A_c \rangle_{II} L_c^2 = C$, a constant. We can thus draw a phase diagram as in figure 6, where, if for a given value of the noise amplitude ΔR the system falls below the transition line, the dislocation is in Region I and $\langle A_c \rangle$ is proportional to $1/L^{1/2}$, while if the system is above the line, the dislocation is in Region II and $\langle A_c \rangle$ is a constant independent of L.

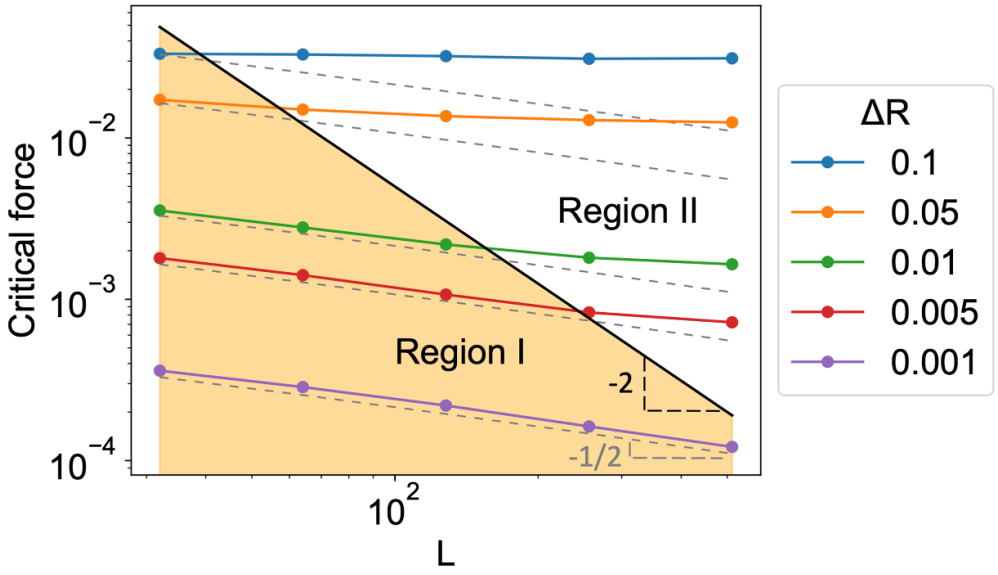

Figure 6. Average critical force as a function of cell size for different noise amplitudes indicated in the legend. Colored lines are results of simulations in cells of size $L \times L$, grey dashed lines are predictions of Larkin model (slope $-1/2$ in this log-log plot) and the back line is the weak-to-strong pinning transition between Regions I and II (slope -2 in this log-log plot). The height of this line was chosen to match the end of Larkin model's validity evidenced in the simulations.

4. Effect of correlations

Now that we have shown the relevance of the Larkin model with a white noise, we can discuss its prediction in the presence of correlations. In [18, 19, 28], we have shown that the stress noise due to random solutes is spatially correlated. Using elasticity theory, we obtained closed-form expressions for the correlation functions of shear stresses in the glide plane of a dislocation. Correlations are anisotropic: a shear stress has a different auto-correlation in the direction of the shear (so-called longitudinal direction) than in the perpendicular direction (transverse direction). Both correlation functions have a $1/r^3$ asymptotic behavior at long range, characteristic of disordered systems [48], but with different signs. In [28], we performed extensive simulations to measure the yield stress as a function of the noise amplitude in Region II of collective pinning. We will see below that a modified Larkin model accounting for stress correlations can predict the result of these simulations.

From equations (6) and (8), the width of a dislocation is expressed in Region I, where Larkin model applies, as:

$$\omega^2 = \sum_{k\neq 0} \frac{\langle |\widehat{R}_k|^2 \rangle}{k^4}, \tag{13}$$

where $\widehat{R}_k$ is the Fourier transform of the solute noise along the dislocation, which depends on the noise correlation. Since the latter is anisotropic, the width depends on the dislocation character, in contrast with a white noise. For an edge dislocation, the Burgers vector and associated plastic shear are perpendicular to the dislocation line. An edge dislocation is thus sensitive to

transverse correlations, while a screw dislocation, which has a Burgers vector parallel to its line, is sensitive to longitudinal correlations. In [28], we provided expressions for the PSD of the noise in the transverse, $\langle|\widehat{R}_k^E|^2\rangle$, and longitudinal directions, $\langle|\widehat{R}_k^S|\rangle$, which correspond to edge and screw dislocations respectively:

$$\langle|\widehat{R}_k^E|^2\rangle = \Delta R^2 \frac{15\sqrt{\pi}}{4L} k^2 \left(e^{-k^2} \left(1 + \frac{1}{k^2}\right) + \left(2 + k^2\right) \mathrm{Ei}\left(-k^2\right) \right) \tag{14}$$

$$\langle|\widehat{R}_k^S|^2\rangle = \Delta R^2 \frac{15\sqrt{\pi}}{L} k^2 \left(-e^{-k^2} - \left(1 + k^2\right) \mathrm{Ei}\left(-k^2\right) \right), \tag{15}$$

with $\mathrm{Ei}(x) = -\int_{-x}^{\infty} \frac{e^{-u}}{u} du$, the integral exponential function. In contrast with the uncorrelated case, the dislocation width cannot be computed exactly for the edge and screw dislocations. However, in the limit $L \gg 1$, we can replace the sum in equation (13) by an integral and express the width of edge and screw dislocations as:

$$\omega_E^2 = \Delta R^2 \frac{15}{8\sqrt{\pi}} \int_{2\pi/L}^{\infty} \frac{1}{k^2} \left(e^{-k^2} \left(1 + \frac{1}{k^2}\right) + \left(2 + k^2\right) \mathrm{Ei}\left(-k^2\right) \right) \mathrm{d}k \tag{16}$$

$$\omega_S^2 = \Delta R^2 \frac{15}{2\sqrt{\pi}} \int_{2\pi/L}^{\infty} \frac{1}{k^2} \left(-e^{-k^2} - \left(1 + k^2\right) \mathrm{Ei}\left(-k^2\right) \right) \mathrm{d}k. \tag{17}$$

We have introduced a cut-off at small k to account for the finite length of the dislocations. Both integrals can be computed analytically, yielding with $K = 2\pi/L$:

$$\omega_E^2 = \Delta R^2 \frac{15}{8\sqrt{\pi}} \left(\frac{e^{-K^2}}{3K^3} + \frac{13e^{-K^2}}{3K} - \frac{16\sqrt{\pi}}{3} \mathrm{erfc}\left(K\right) - \left(K - \frac{2}{K}\right) \mathrm{Ei}\left(-K^2\right) \right) \tag{18}$$

$$\omega_S^2 = \Delta R^2 \frac{15}{2\sqrt{\pi}} \left(-\frac{e^{-K^2}}{3K} + 4\sqrt{\pi}\mathrm{erfc}\left(K\right) + \left(K - \frac{1}{K}\right) \mathrm{Ei}\left(-K^2\right) \right). \tag{19}$$

From the asymptotic behavior $\mathrm{Ei}(-K^2) \sim \gamma_e + 2\log(K)$ when $K \to 0$ (γ_e is the Euler–Mascheroni constant), and keeping only the leading terms, we have:

$$\omega_E^2 = \Delta R^2 \frac{5}{8\sqrt{\pi}} \frac{1}{K^3}, \tag{20}$$

$$\omega_S^2 = \Delta R^2 \frac{15}{\sqrt{\pi}} \frac{-\log\left(K\right)}{K}. \tag{21}$$

We see that the Larkin lengths of the edge and screw dislocations (such that $\omega_{E/S} = 1$) depend differently on the noise amplitude:

$$L_{c,E} \propto 1/\Delta R^{2/3} \tag{22}$$

$$L_{c,S}/\log\left(L_{c,S}\right) \propto 1/\Delta R^2. \tag{23}$$

The Larkin length of the edge dislocation has the same $1/\Delta R^{2/3}$ scaling as with a white noise (see equation (9)), while the screw dislocation has a different scaling. Note that in [28], we expressed the Larkin length from an equilibrium between line tension and stress noise and

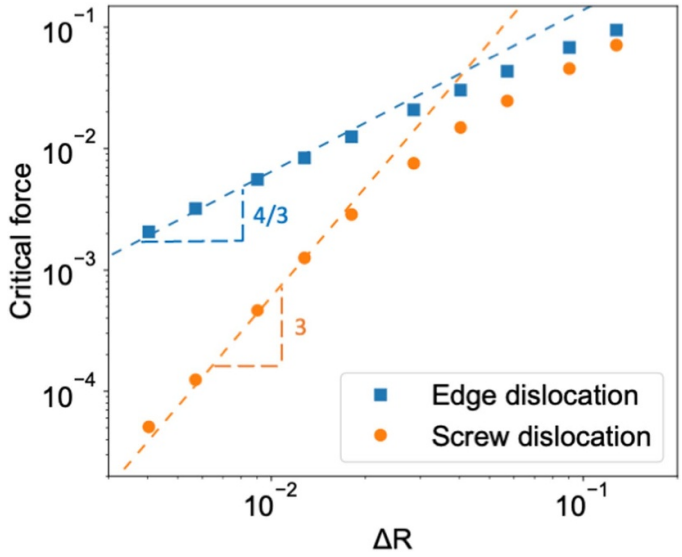

Figure 7. Average critical force on edge and screw dislocations as a function of noise amplitude in presence of noise correlations and extrapolated to infinite cell sizes.

obtained the same scaling for the edge dislocation but a different scaling for the screw dislocation ($L_{c,S} \propto 1/\Delta R$). The way to define the Larkin length thus matters when correlations are accounted for.

Still following the Larkin model, we express the critical force in Region II as the average random force on a segment of length L_c. In [28], we provided expressions for the variance of this random force, $F_E \propto \Delta R/\sqrt{L_{c,E}}$ for the edge dislocation and $F_S \propto \Delta R/L_{c,S}$ for the screw dislocation. Equating the latter with the critical force and using the scaling of L_c with ΔR, we obtain:

$$\langle A_c \rangle_{II,E} \propto \Delta R^{4/3} \tag{24}$$

$$\langle A_c \rangle_{II,S} \propto \Delta R^{3}, \tag{25}$$

where for the screw dislocation, we neglected the logarithmic correction in equation (23). Very interestingly, we see that due to the correlations of the stress noise, the yield stresses of edge and screw dislocations scale differently with ΔR.

In figure 7, we show a comparison between line tension simulations in correlated noises for edge and screw dislocations and the scaling laws obtained above. The simulations were published in [28]. They were performed in cells of different sizes with a grid size small enough to reproduce the spatial correlations of the stress field. The simulations were then numerically extrapolated to infinite systems. The simulations confirm that the yield stress of an edge dislocation has the same scaling as with a white noise, as predicted above. The screw dislocation, on the other hand, shows a different scaling, which again agrees with our prediction, at least at low noise amplitude. This confirms the validity of our approach and the definition of the Larkin length.

5. Application to atomistic calculations

In order to support our analysis, we compare in this last part the predictions of the model with static computations carried out at the atomic scale. We study the yield stress of dislocations via atomistic calculations in two model face-centered cubic (FCC) alloys of Ni(Al) and Al(Mg). These systems were studied in detail in [49–52] by systematically comparing the variation of the yield stress as a function of the concentration of solute atoms for screw and edge dislocations. Until now, core effects, such as the lattice friction characteristic of screw dislocations, have not been taken into account in our theoretical analysis. We therefore focus here on edge dislocation, whose Peierls stress is negligible compared to solute pinning.

In the case of an edge dislocation in the Ni(Al) alloy, it has been shown that the paradigm of the depinning transition of an elastic interface in a random medium applies to atomic scale simulations [35]. The propagation of a dislocation in a field of random solutes is governed by avalanches whose spatial extension and intermittency diverge characteristically at the critical threshold. Their shape can be described from scalings characterized by critical exponents, thus confirming again the difficulty in geometrically identifying any characteristic length in atomistic configurations.

Unlike line tension simulations where the noise amplitude is set *a priori*, the anchoring of dislocations emerges naturally from the interaction between the dislocations and the solutes. Its physical origin comes from the mismatch in size and moduli between the solutes and the matrix. At short range, barriers to dislocation motion also involve nonlinear interactions with the dislocation core and the stacking fault ribbon in FCC metals. In this context, the advantage of atomistic simulations is that they automatically take into account this complexity in a realistic way, including the effects of the spatial correlations of the stress field discussed in the previous section.

The price to pay for the exhaustive description of this complexity lies in the prohibitive increase in the number of degrees of freedom compared to the line tension model. This is particularly the case for dislocations, which involve long-range elastic interactions. In order to remedy these difficulties, we rely on a classical method consisting of applying periodic boundary conditions in the direction of slip (direction y) and along the dislocation line (direction x), while in the z direction, modified free boundary conditions are used with external forces to apply a τ_{yz} shear stress [53].

However, this method does not make it possible to completely dissociate the size effect of statistical origin discussed in this work from the effect coming from dislocation rigidity. The elastic energy of a straight isolated dislocation varies indeed as the logarithm of the size of the system in the direction perpendicular to the dislocation line. The boundary conditions further imply an interaction of the dislocation with its periodic images and those due to the free surfaces. These image dislocations thus amount to simulate an infinite array of dislocations separated by L_y in a thin section of thickness L_z. Under these conditions, only the length L_x of the system will be varied to study the effect of the size of the system on the critical stress while maintaining a constant line tension.

We simulate a single edge dislocation in a dense plane $\{111\}$. The system size is chosen so that the spreading of the dislocation cores does not change qualitatively for larger sizes. We use $L_y = 40b$ in the glide direction, and a separation between free surfaces of $L_z = 16b$. The length in the direction of the dislocation line L_x varies from $7b$ to $520b$. Once the dislocation is introduced into the crystal, we randomly substitute atoms in the matrix with solutes. Three

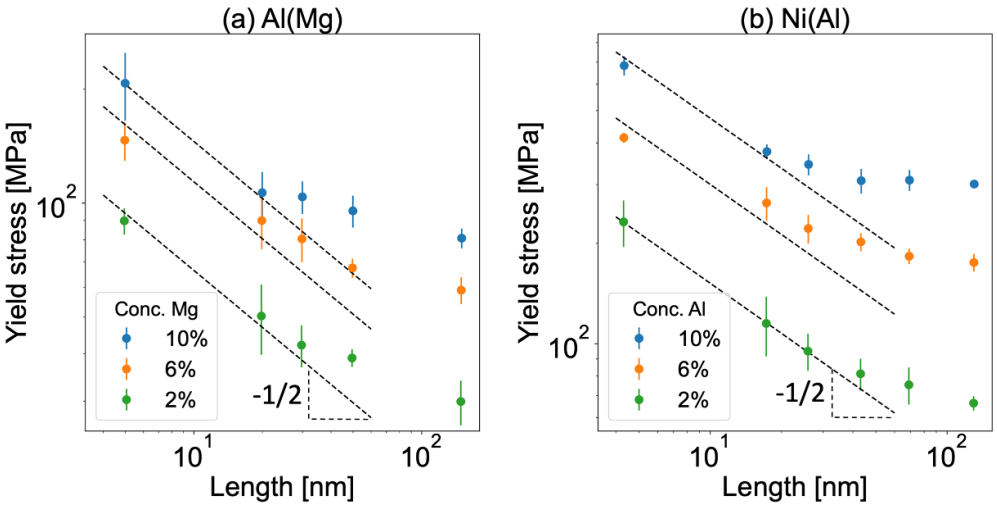

Figure 8. Average yield stress of edge dislocations in (a) Al(Mg) and (b) Ni(Al) solid solutions measured by atomistic simulations. Mean yield stresses and standard deviations were obtained by sampling from five different cells.

concentrations are investigated: 2, 6 and 10%. The lattice parameter varies as a function of the solute concentration following Vegard's linear law.

After a first relaxation of the system's potential energy, we apply a stress on the z surfaces of the crystal in increments of 4 MPa. After each increment, the system is relaxed until the dislocation finds a stable position or glides up to a certain gliding distance. When the dislocation glides, it may cross the simulation box several times due to the periodic conditions. At each pass, the dislocation shears the crystal and shifts the crystal above the glide plane by a Burgers vector relative to the crystal below the glide plane, thus creating a new distribution of solute atoms. The positions taken by the dislocation in the sliding direction along the dislocation line are not identical on each pass through the simulation box. We, therefore, simulate the equivalent of the sliding of a dislocation in an extended solid solution whose distribution of obstacles is random to first approximation.

The dislocation no longer finds a stable configuration above a critical stress, which corresponds to the yield stress. Its value depends on the distance traveled by the dislocation. The greater the distance the dislocation travels, the greater the probability of encountering an pinning configuration. We choose a minimum glide distance of $400b$, i.e. about 10 simulation box lengths. All calculations are averaged over five realizations for each concentration.

We present in figure 8 atomistic calculations of the yield stress of edge dislocations in model Ni(Al) and Al(Mg) solid solutions. We observe that the elastic limit increases with the solute atom concentration. Moreover, we see that in both solid solutions, the yield stress decreases rapidly at small dislocation lengths, with the $L_x^{-1/2}$ scaling expected from the above analysis. At longer dislocation lengths, there is a crossover to a regime where the size dependence is much weaker. However, the yield stress does not converge to a finite value but continues to decrease as expected since, with a fixed glide distance, the yield stress of an infinitely long dislocation is zero. More data would be required for a detailed analysis, but the crossover between strong and weak size dependence clearly shows the existence of a Larkin length for each alloy composition.

6. Conclusions

To answer the somewhat provocative title of this article, we can say that, yes, the Larkin length exists. However, it is not a dominant length scale allowing the decomposition of dislocations into straight segments of length L_c nor into a sine wave of wavelength L_c. Instead, the Larkin length is a crossover length in at least three facets of dislocation behavior: (1) the dislocation width exceeds the noise correlation above L_c, (2) the yield stress becomes size-independent, and (3) the PSD changes scaling.

Other definitions of Larkin length have been proposed. For instance, in [54], the Larkin length is defined as the first root of the height-height autocorrelation function along the dislocation, i.e. as an estimate of the correlation length of the dislocation height [55]. This definition does not seem appropriate for several reasons. First, it is strongly anchored on a sinusoidal approximation of the dislocation line, which we have seen is not justified. Second, we checked that at least with the line tension model, the first root of the correlation function scales with the dislocation length L, which contradicts the notion of a characteristic length scale.

On a final note, the present analysis suggests a practical methodology for predicting yield stresses within atomistic models. The first step involves conducting simulations in small square cells of varying dimensions below L_c to determine the scaling laws governing the dislocation width and yield stress. By applying the scaling law for the width, L_c can be determined, such that $\omega(L_c) = a_C$, where a_C should scale with the correlation length of the noise. a_C will correspond to a fraction of the separation between energy valleys, which can be determined by relaxing a dislocation at different positions in a cell. Within the line tension model, we have found an average separation between equilibrium positions $d \simeq 4a$, independently of L and ΔR, thus suggesting to use $a_C = d/4$. With L_c known, the scaling law of the yield stress can be used to extrapolate the latter to L_c. This yield stress corresponds directly to the thermodynamic limit since beyond L_c, the yield stress is size-independent. We have successfully demonstrated the effectiveness of this approach for a line tension model in the presence of both uncorrelated and correlated noise. Verification of this methodology with more complex models, including atomistic simulations, is currently in progress. We may expect complications related to core effects, i.e. short-range interactions of the solutes in direct contact with the dislocation line, that may affect the core structure [56–58]. But the notion of a crossover length controlling the dislocation behavior should be robust.

Data availability statement

The data that support the findings of this study are openly available at the following URL/DOI: https://ilm-perso.univ-lyon1.fr/ drodney/.

Acknowledgments

The authors thank Ronan Madec for his help in illustrating early and current dislocation dynamics simulations. Fruitful discussions with Dr C Varvenne are also warmly acknowledged.

ORCID iDs

David Rodney https://orcid.org/0000-0001-5311-0754
Pierre-Antoine Geslin https://orcid.org/0000-0001-9549-7889

References

[1] Estrin Y, Brechet Y, Sevillano J G and Madec R 2023 Obituary Ladislas Kubin Acta Mat. **246** 118690
[2] Kubin L 2013 *Dislocations, Mesoscale Simulations and Plastic Flow* vol 5 (Oxford University Press)
[3] Louchet F and Kubin L 1975 Dislocation substructures in the anomalous slip plane of single crystal niobium strained at 50 K *Acta Metall.* **23** 17–21
[4] Lebyodkin M, Brechet Y, Estrin Y and Kubin L 1995 Statistics of the catastrophic slip events in the Portevin–Le Châtelier effect *Phys. Rev. Lett.* **74** 4758
[5] Bharathi M, Lebyodkin M, Ananthakrishna G, Fressengeas C and Kubin L 2001 Multifractal burst in the spatiotemporal dynamics of jerky flow *Phys. Rev. Lett.* **87** 165508
[6] Madec R, Devincre B, Kubin L, Hoc T and Rodney D 2003 The role of collinear interaction in dislocation-induced hardening *Science* **301** 1879–82
[7] Devincre B, Hoc T and Kubin L 2008 Dislocation mean free paths and strain hardening of crystals *Science* **320** 1745–8
[8] Ghoniem N M and Amodeo R 1988 Computer simulaltion of dislocation pattern formation *Solid State Phenom.* **3** 377–88
[9] Kubin L, Estrin Y and Canova G 1990 Dislocation patterns and plastic instabilities *Patterns, Defects and Materials Instabilities* (Springer) pp 277–301
[10] Madec R and Kubin L P 2017 Dislocation strengthening in fcc metals and in bcc metals at high temperatures *Acta Mater.* **126** 166–73
[11] Devincre B and Condat M 1992 Model validation of a 3D simulation of dislocation dynamics: discretization and line tension effects *Acta Metall. Mater.* **40** 2629–37
[12] Saada G 1960 Sur le durcissement dû à la recombinaison des dislocations *Acta Metall.* **8** 841–7
[13] Rodney D and Phillips R 1999 Structure and strength of dislocation junctions: an atomic level analysis *Phys. Rev. Lett.* **82** 1704
[14] Foreman A and Makin M 1966 Dislocation movement through random arrays of obstacles *Phil. Mag.* **14** 911–24
[15] Nogaret T and Rodney D 2006 Finite-size effects in dislocation glide through random arrays of obstacles: line tension simulations *Phys. Rev.* B **74** 134110
[16] Legros M 2014 In situ mechanical TEM: seeing and measuring under stress with electrons *C. R. Physique* **15** 224–40
[17] Geslin P-A 2024 Modeling of solid solution strengthening in FCC alloys: atomistic simulations, statistical models and elastic continuous approaches *Comput. Mater. Sci.* **232** 112624
[18] Geslin P-A and Rodney D 2021 Microelasticity model of random alloys. Part I: mean square displacements and stresses *J. Mech. Phys. Solids* **153** 104479
[19] Geslin P-A, Rida A and Rodney D 2021 Microelasticity model of random alloys. Part II: displacement and stress correlations *J. Mech. Phys. Solids* **153** 104480
[20] Nattermann T, Stepanow S, Tang L-H and Leschhorn H 1992 Dynamics of interface depinning in a disordered medium *J. Phys.* II **2** 1483–8
[21] Leschhorn H 1993 Interface depinning in a disordered medium-numerical results *Physica* A **195** 324–35
[22] Barabási A-L *et al* 1995 *Fractal Concepts in Surface Growth* (Cambridge University Press)
[23] Rosso A and Krauth W 2001 Origin of the roughness exponent in elastic strings at the depinning threshold *Phys. Rev. Lett.* **87** 187002
[24] Agoritsas E, Lecomte V and Giamarchi T 2012 Disordered elastic systems and one-dimensional interfaces *Physica* B **407** 1725–33
[25] Ferrero E E, Bustingorry S and Kolton A B 2013 Nonsteady relaxation and critical exponents at the depinning transition *Phys. Rev.* E **87** 032122
[26] Bolech C J and Rosso A 2004 universal statistics of the critical depinning force of elastic systems in random media *Phys. Rev. Lett.* **93** 125701
[27] Budrikis Z and Zapperi S 2013 Size effects in dislocation depinning models for plastic yield *J. Stat. Mech.* 04029
[28] Rida A, Martinez E, Rodney D and Geslin P-A 2022 Influence of stress correlations on dislocation glide in random alloys *Phys. Rev. Mater.* **6** 033605
[29] Larkin A I 1970 Effect of inhomogeneties on the structure of the mixed state of superconductors *Sov. J. Exp. Theor. Phys.* **31** 784

[30] Larkin A and Ovchinnikov Y N 1979 Pinning in type II superconductors *J. Low Temp. Phys.* **34** 409–28
[31] Zapperi S and Zaiser M 2001 Depinning of a dislocation: the influence of long-range interactions *Mater. Sci. Eng.* A **309** 348–51
[32] Zaiser M 2002 Dislocation motion in a random solid solution *Phil. Mag.* A **82** 2869–83
[33] Zhai J-H and Zaiser M 2019 Properties of dislocation lines in crystals with strong atomic-scale disorder *Mater. Sci. Eng.* A **740** 285–94
[34] Péterffy G, Ispánovity P D, Foster M E, Zhou X and Sills R B 2020 Length scales and scale-free dynamics of dislocations in dense solid solutions *Mater. Theory* **4** 1–25
[35] Patinet S, Bonamy D and Proville L 2011 Atomic-scale avalanche along a dislocation in a random alloy *Phys. Rev.* B **84** 174101
[36] Sevillano J G, Bouchaud E and Kubin L 1991 The fractal nature of gliding dislocation lines *Scr. Metall. Mater.* **25** 355–60
[37] Leyson G P M, Curtin W A, Hector L G Jr Woodward C F 2010 Quantitative prediction of solute strengthening in aluminium alloys *Nat. Mater.* **9** 750–5
[38] Varvenne C, Leyson G P M, Ghazisaeidi M and Curtin W A 2017 Solute strengthening in random alloys *Acta Mater.* **124** 660–83
[39] Démery V, Rosso A and Ponson L 2014 From microstructural features to effective toughness in disordered brittle solids *Europhys. Lett.* **105** 34003
[40] Bustingorry S, Kolton A and Giamarchi T 2010 Random-manifold to random-periodic depinning of an elastic interface *Phys. Rev.* B **82** 094202
[41] Bitzek E, Koskinen P, Gähler F, Moseler M and Gumbsch P 2006 Structural relaxation made simple *Phys. Rev. Lett.* **97** 170201
[42] Rosso A and Krauth W 2002 Roughness at the depinning threshold for a long-range elastic string *Phys. Rev.* E **65** 025101
[43] Patinet S, Vandembroucq D and Roux S 2013 Quantitative prediction of effective toughness at random heterogeneous interfaces *Phys. Rev. Lett.* **110** 165507
[44] Tanguy A and Vettorel T 2004 From weak to strong pinning I: a finite size study *Eur. Phys. J.* B **38** 71–82
[45] Leyson G and Curtin W 2013 Friedel vs. labusch: the strong/weak pinning transition in solute strengthened metals *Phil. Mag.* **93** 2428–44
[46] Gumbel E J 1958 *Statistics of Extremes* (Columbia University Press)
[47] Leyson G and Curtin W 2016 Solute strengthening at high temperatures *Modelling Simul. Mater. Sci. Eng.* **24** 065005
[48] Lemaître A 2018 Stress correlations in glasses *J. Chem. Phys.* **149** 104107
[49] Proville L, Rodney D, Brechet Y and Martin G 2006 Atomic-scale study of dislocation glide in a model solid solution *Phil. Mag.* **86** 3893–920
[50] Patinet S and Proville L 2008 Depinning transition for a screw dislocation in a model solid solution *Phys. Rev.* B **78** 104109
[51] Proville L and Patinet S 2010 Atomic-scale models for hardening in FCC solid solutions *Phys. Rev.* B **82** 054115
[52] Patinet S and Proville L 2011 Dislocation pinning by substitutional impurities in an atomic-scale model for Al(Mg) solid solutions *Phil. Mag.* **91** 1581
[53] Bacon D, Osetsky Y N and Rodney D 2009 Dislocation–obstacle interactions at the atomic level *Dislocations in Solids* vol 15 (Elsevier) pp 1–90
[54] Antillon E, Woodward C, Rao S, Akdim B and Parthasarathy T 2019 A molecular dynamics technique for determining energy landscapes as a dislocation percolates through a field of solutes *Acta Mater.* **166** 658–76
[55] Rao S I, Woodward C, Parthasarathy T A and Senkov O 2017 Atomistic simulations of dislocation behavior in a model FCC multicomponent concentrated solid solution alloy *Acta Mater.* **134** 188–94
[56] Yu Q, Qi L, Tsuru T, Traylor R, Rugg D, Morris J Jr, Asta M, Chrzan D and Minor A M 2015 Origin of dramatic oxygen solute strengthening effect in titanium *Science* **347** 635–9
[57] Buey D, Hector L Jr and Ghazisaeidi M 2018 Core structure and solute strengthening of second-order pyramidal $\langle c+a \rangle$ dislocations in mg-y alloys *Acta Mater.* **147** 1–9
[58] Lüthi B, Ventelon L, Rodney D and Willaime F 2018 Attractive interaction between interstitial solutes and screw dislocations in bcc iron from first principles *Comput. Mater. Sci.* **148** 21–26